Bio-Medical Materials and Engineering 26 (2015) S729–S738
DOI 10.3233/BME-151364
IOS Press

Biomechanical modeling and load-carrying simulation of lower limb exoskeleton

Yanhe Zhu*, Guoan Zhang, Chao Zhang, Gangfeng Liu and Jie Zhao
State Key Laboratory of Robotics Institute, Science Park Robotics Institute, Harbin Institute of Technology, Heilongjia 150006, China

Abstract. This paper introduces novel modern equipment— a lower extremity exoskeleton, which can implement the mutual complement and the interaction between human intelligence and the robot's mechanical strength. In order to provide a reference for the exoskeleton structure and the drive unit, the human biomechanics were modeled and analyzed by LifeModeler and Adams software to derive each joint kinematic parameter. The control was designed to implement the zero-force interaction between human and exoskeleton. Furthermore, simulations were performed to verify the control and assist effect. In conclusion, the system scheme of lower extremity exoskeleton is demonstrated to be feasible.

Keywords: Lower extremity exoskeleton, controller, zero-force interaction, simulation

1. Introduction

Compared to other robots, lower extremity exoskeletons possess obvious advantages toward improving the capability and efficiency of workers and soldiers [1, 2]. Moreover, with the development of the exoskeleton, both the operational modes and the types are extended by foreign countries [3-5]. In 2004, engineers from the University of California, Berkeley presented the Berkeley Lower Extremity Exoskeleton (BLEEX), designed to assist people in load-bearing walking. Although BLEEX was outstanding in many aspects, its weight and load-bearing capacity could not meet military demands [6]. The Human Universal Load Carrier (HULC) was later presented by the University of California Berkeley as an improvement of BLEEX. Following a similar trend, researchers at Tsukuba University, Japan, introduced Hybrid Assistive Limb (HAL), an electrically-actuated whole-body exoskeleton [7-9]. Also in Japan, the Kanagawa University proposed wearable power suit, which can greatly expand physical capability [10].

In response to this growing trend in domestic exoskeleton development, there are numerous laboratories engaging in this research [11]. However, there is still a wide deviation between experimental and practical applications.

Lower extremity exoskeletons utilize a wide range of applied sciences, including robotics, ergonomics, bionics and control theory. Therefore, many factors must be taken into account to address the

* Address for correspondence: Yanhe Zhu, State Key Laboratory of Robotics Institute, Harbin Institute of Technology, HIT Science Park Robotics Institute 203, Yikuang Street No. 2, Nangang District, Harbin, Heilongjia 150006, China. Tel.: 13074594165; Fax: 0451-86414538; E-mail: yhzhu@hit.edu.cn.

wearer's movement and assisting effect. Exoskeleton research can be categorized into the following analyses: I) anthropomorphic structural design; II) human gait analysis; III) accuracy of the detection system; IV) rationality of the driving method; V) response characteristics of the control system.

The contribution of this paper is as follows: through LifeModeler and Adams software, the body model has been designed utilizing an innovative method which includes the positive and inverse dynamics simulation to achieve a muscle model, improving the accuracy of gait parameters and muscle torques. The control system and dynamic equation were derived from the data obtained. Finally, wearing simulation analysis proved that the control system exhibits improved response characteristics, and exoskeleton design is feasible.

2. Structure design

Due to the physical contact between the exoskeleton and the human body, comfort and safety are primary considerations. Therefore, the anthropomorphic design is the prerequisite to wearing comfort and safety. The exoskeleton structure determines not only its range of movement, but also the wearing comfort; moreover, it is the premise of the zero-force interaction design. Figure 1 is an overall model, simplified to emphasize the major design components. Figure 2 is a representation of the experimental platform.

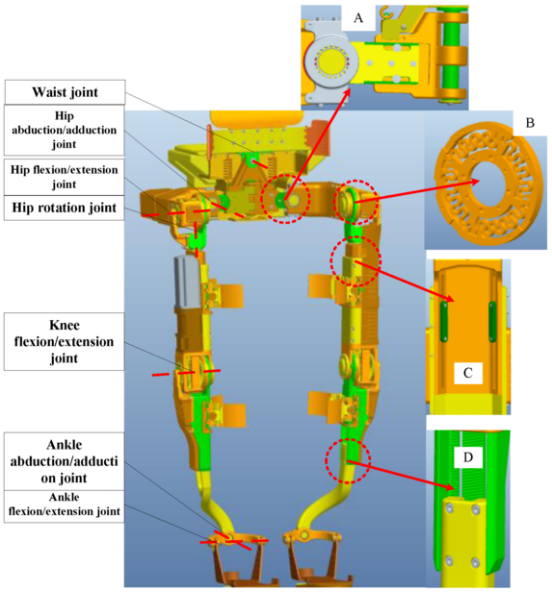

Fig. 1. Exoskeleton model, The hip has 3 dof; the knee has 1 dof; the ankle has 2 dof; the waist has 1 dof; A/C/D represents the adjustment, B represents the elastic element; the actuators are present in the hip and knee.

Fig. 2. Experimental platform.

BODY MEASUREMENT TABLE (length data displayed in inches)

Male Female Child Non-Human Hands Gripping Hands Open

Age (months)	240.0	Waist_Depth	8.581	Left Knee Ht Seated	21.606
Weight (lbs)	165.343	Waist Breadth	11.913	Right Thigh Circum.	22.673
Standing_Height	68.897	Buttock Depth	9.226	Left Thigh Circum.	22.673
Right Shoulder Ht	56.309	Hip Breadth Standing	13.653	Right Upper Leg Circum.	14.959
Left Shoulder Ht	56.309	Right Shoulder To Elbow Ln	13.963	Left Upper Leg Circum.	14.959
Right Armpit Ht	50.350	Left Shoulder To Elbow Ln	13.963	Right Knee Circum.	15.198
Left Armpit Ht	50.350	Right Forearm Hand Length	19.196	Left Knee Circum.	15.198
Waist Height	41.296	Left Forearm Hand Length	19.196	Right Calf Circum.	14.405
Seated Height	36.297	Right Biceps Circumference	12.180	Left Calf Circum.	14.405
Head_Length	7.789	Left Biceps Circumference	12.180	Right Ankle Circum.	8.694
Head_Breadth	6.116	Right Elbow Circum.	12.129	Left Ankle Circum.	8.694
Head To Chin Ht	8.921	Left Elbow Circum.	12.129	Right Ankle Ht Outside	5.324
Neck Circum.	14.918	Right Forearm Circum.	10.928	Left Ankle Ht Outside	5.324
Shoulder Breadth	19.050	Left Forearm Circum.	10.928	Right Foot Breadth	3.801
Chest Depth	9.468	Right Wrist Circum.	6.83	Left Foot Breadth	3.801
Chest Breadth	12.688	Left Wrist Circum.	6.83	Right Foot Length	10.511
		Right Knee Ht Seated	21.606	Left Foot Length	10.511

Fig. 3. The parameters of the human body model.

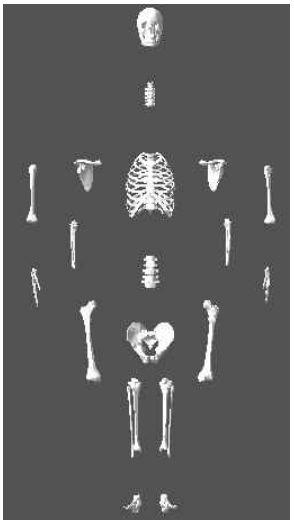

Fig. 4. The rigid-body model.

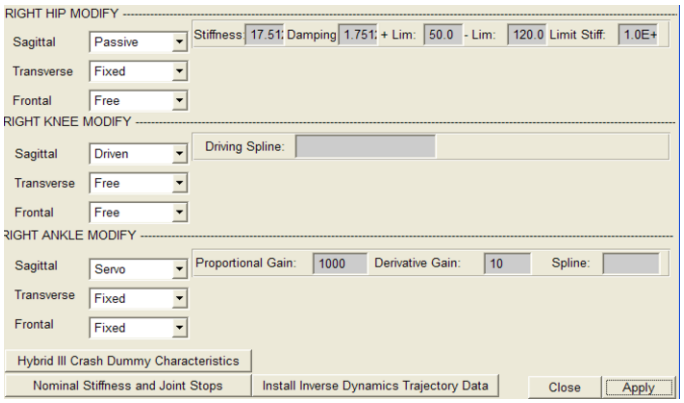

Fig. 5. Joint parameters.

3. Biomechanical modeling

3.1. Hardware and software

LifeModeler modeling system is employed for this analysis [12-14]. The LifeModeler model is designed to support a 20-year-old, 75kg and 175cm Chinese man. Figure 3 exhibits the parameters of the human body model. Figure 4 demonstrates the rigid-body model.

In this analysis, the human joints are equivalent to hinges; the specific parameters are shown in Figure 5.

3.2. Simulation method design

Human level walking is utilized for gait analysis [15, 16]. Five types of experiment are executed: I) Utilizing gait measurements to acquire the space position of various marked points in human level

walking. II) Establishment of the level walking model via LifeModeler software. III) Inverse dynamics simulation based on the mode of traction, as illustrated in Figure 6; the walking model is determined by the marked point motion curves, generated by practical motion data or user input, to record the changes in joint angles. IV) Positive dynamics simulation to generate a muscle motion model according to the joint angles recorded in the inverse dynamics simulation; the muscle learning element or passive motion element becomes invalid, and turns to shrinkage element in order to record the change of the muscle length. V) By data of the muscle changing, the muscle drives the model to remove actively.

3.3. Muscle modeling

Since the skeleton movement of the human body is activated by muscle contraction and stretching, muscle mechanical properties and functions are necessary to the analysis of biomechanics in relation to human movement. However, the mechanical properties of human muscle are very complicated. They are not only related to the mechanical properties of physical media which constitutes the muscle, but are also affected by the excitement and fatigue states of the muscle. In order to illustrate the mechanical properties of human muscle, Archibald Vivian Hill British biophysicist and winner of the Nobel Prize in Physiology or Medicine, proposed the three-element model of muscle structure, as shown in Figure 7.

Since the force is only produced when the muscle is being stretched, the power of each muscle is finite; the function expression of the muscle force is set up in Eq. (1)

$$F_1 = \begin{cases} F_{\max} & : if\ F_1 \geq F_{\max} \\ P_{gain}(L_{desired} - L_{actual}) + D_{gain}(\dot{L}_{desired} - \dot{L}_{actual}) & : if\ F_1 < F_{\max} \\ 0 & : if\ L_{desired} \geq L_{actual} \end{cases} \tag{1}$$

$$F_i = F_{filter}(F_1) \tag{2}$$

In Eq. (2), F_{filter}——weight coefficient, is used to adjust the percentage of output power in each muscle, $0 \leq F_{filte} \leq 200\%$.

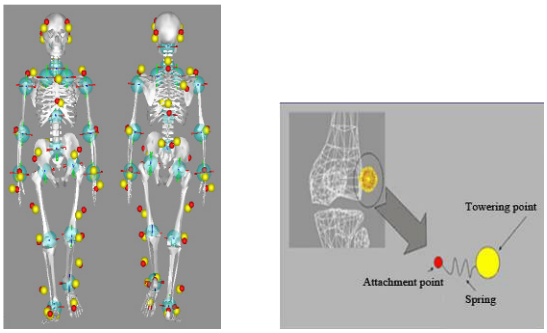

Fig. 6. Traction moving model. Towing points are identified in yellow, attachment points are in red. Both are connected by the bushing element which can produce force and torque in three dimensions. This traction method enables the simulation to avoid geometric error between the simulation model and the test subject, and position error between the marked points.

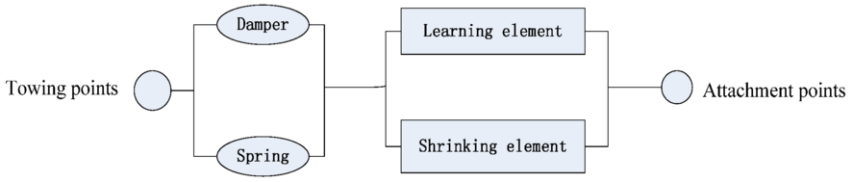

Fig. 7. Hill's muscle model. The entire muscle consists of the series elastic element, parallel elastic element and construction element. The muscle mechanical properties are determined by the system of these three elements. In these elements, the parallel elastic element represents the thickness of the muscle; the series elastic element represents the length of the muscle.

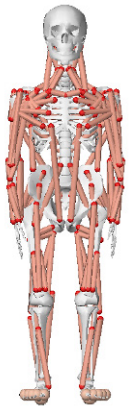

Fig. 8. Muscle model.

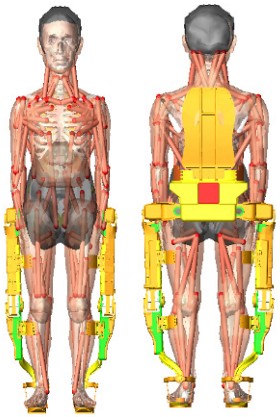

Fig. 9. Human-exoskeleton hybrid model.

F_{max}——maximum output power, $F_{max}=pCSA \cdot M_{stress}$ ($pCSA$: physiological cross sectional area ; M_{stress}: maximum tissue stress)

The final muscle model is shown in Figure 8.

3.4. Constraint relation modeling

The Human-exoskeleton collaborative movement simulation combines the human and exoskeleton models. Figure 9 illustrates the human-exoskeleton hybrid model. In order to ensure the accuracy of the simulation result, the simulation model and practical model are as identical as possible. Moreover, the constraints between human and exoskeleton directly determine their interaction. To facilitate subsequent simulation, the contact model between human and exoskeleton first needs to be established, as shown in Figure 10.

4. Controller design

The exoskeleton robot is a human-machine interaction system, which can obtain the human body movement intentions through the testing system [17]. In essence, it implements a tracking process. Therefore, this chapter begins from the simplest single-joint movement system model, illustrated in Figure 11. In the model, the shank accomplishes active movement and the exoskeleton, represented by a connecting rod, accomplishes the following movement. The purpose of this section is to develop a control strategy which can make the exoskeleton follow human leg movement.

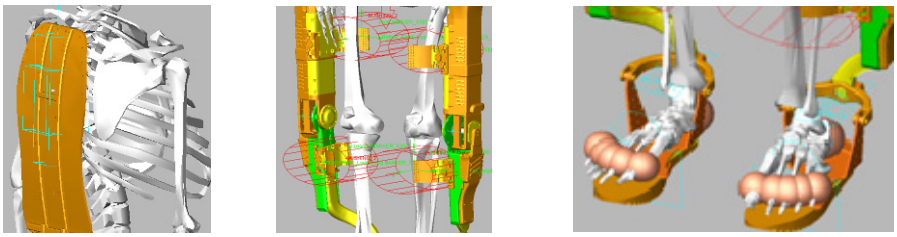

(a) (b) (c)

Fig. 10. (a) The connection method between exoskeleton back and body model. (b) The connection method between exoskeleton leg and body model. (c) The connection method on the soles of the feet. Because the wearer and the exoskeleton robot prototype are connected through belts in the shoulder and waist, the shifting pairs are set between the exoskeleton and the wearer in the simulation model, as shown in Figure 10(a). Along the leg, bundling devices connect the exoskeleton and the human body with bushing units, as shown in Figure 10(b). At the foot, the exoskeleton and the wearer are connected by a belt, allowing some displacement, and represented by fixed constraints in the simulation, as shown in Figure 10(c).

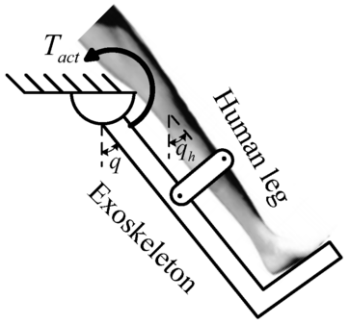

Fig. 11. Single joint.

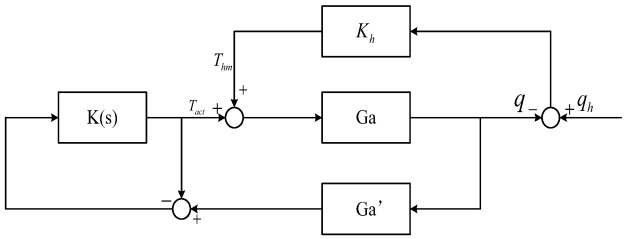

Fig. 12. Closed loop control system.

Figure 12 illustrates the closed loop control system in which K_h represents impedance between the exoskeleton and the body; T_{hm} represents human torque affecting the exoskeleton; Ga represents the system transfer function model; q. represents the joint angle of the exoskeleton; q_h represents the joint angle of the human body; and T_{act} refers to the torque generated by the actuator. The control target $T_{hm} = 0$ is equivalent to $q_h = q$..

In Figure 12, GaGa '= 1, $K(s)=k_p+k_d s$. After a series of derivations, the relationship between the actual joint angle and the ideal joint angle is as follows:

$$\frac{q}{q_h} = \frac{K_h G_a}{1 - K_L + K_h G_a} \tag{3}$$

According to Eq. (3), when $K_L \to 1$, $q \to q_h$, $T_{hm} \to 0$, resulting in zero-force interaction between the wearer and the exoskeleton robot.

What has been discussed above is a one-dimensional system. For the multidimensional system, the dynamic equation can be expressed:

$$M(q)\ddot{q} + C(q,\dot{q})\dot{q} + G(q) = K_h(q_h - q) + T_{act} \tag{4}$$

According to the linearization method of single-degree system, the multidimensional system can be applied in the same way, $T_{act} = K_p T_{hm} + K_d \dot{T}_{hm} + G(q)$. Applied to Eq. (4), we can determine Eq. (5):

$$M(q)\ddot{q} + C(q,\dot{q})\dot{q} = K_h(I + K_p)(q_h - q) + K_h K_d(\dot{q}_h - \dot{q}) \tag{5}$$

5. Simulation

The anthropomorphic design requires the exoskeleton to reflect the movement characteristics of the body, including the scope of activity and the torque of joints. The simulation can facilitate not only the analysis of gait route and joint output curves under the different conditions, but also the structural and controller designs.

5.1. Load-carrying simulation without exoskeleton

Based on the above research, the Adams software is employed for this simulation. Furthermore, the human body model is established and the load-carrying and the non-load-carrying conditions are simulated respectively. Figure 13 illustrates the simulation animation of the non-load-carrying condition; Figure 14 illustrates the load-carrying condition.

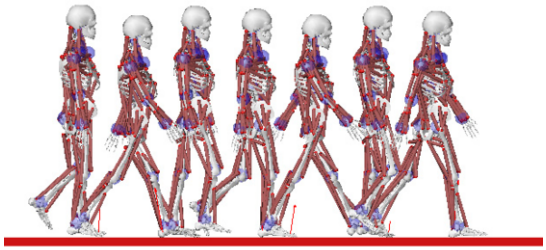

Fig. 13. Illustration of non-load-carrying condition, demonstrating the three stages of a level walking gait cycle: single leg support phase, single leg support redundant phase and legs support phase. The single leg support phase and the legs support phase are collectively referred to as the support phase, accounting for 80% of the gait cycle. The simulation experiment determined: the hip range of flexion/extension is -20°~25°, abduction/adduction is -5°~15°, external/internal rotation is -10°~5°; the knee, range of flexion/extension is -8°~35°; the ankle range of flexion/extension is -5°~13°, abduction/adduction is -2°~2°, external/internal rotation is -8°~2°.

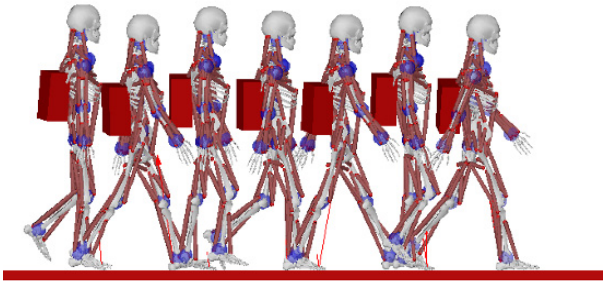

Fig. 14. Illustration of load-carrying condition.

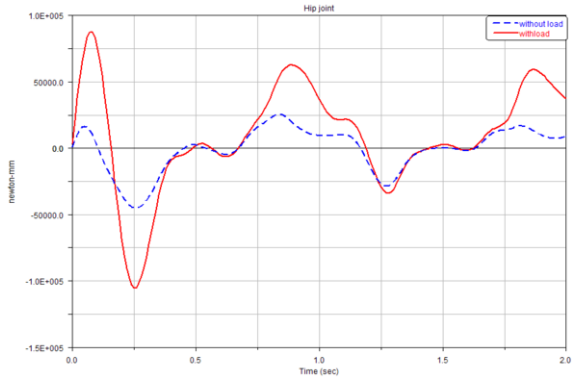

(a) Hip torque curve.

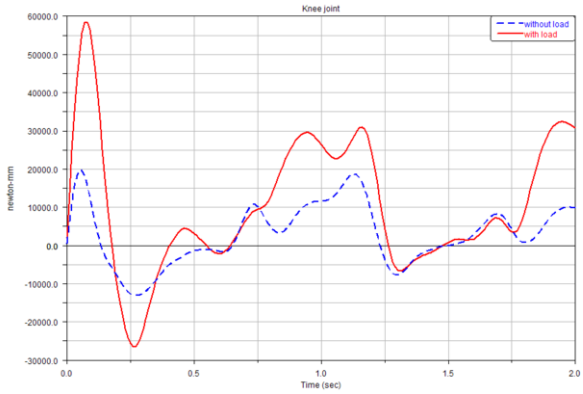

(b) Knee torque curve.

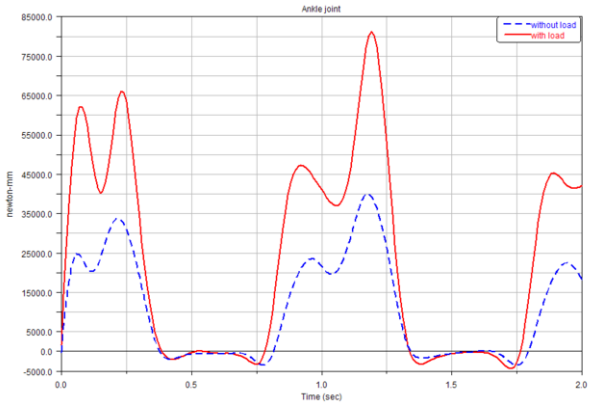

(c) Ankle torque curve.

Fig. 15. Lower body torque curves. The solid line represents the load-carrying simulation curve, and the dotted line represents the non-load-carrying simulation curve. Analysis of the torque curve reveals that in the non-load-carrying simulation, the output of the hip joint torque is the largest while the output of the knee joint torque is the smallest, reaching 45 N·m and 20 N·m, respectively. In the load-carrying simulation, the maximum output of the hip joint torque is approximately 100 N·m, while the maximum torque output of the knee and ankle also reaches 60 N·m and 80 N·m, respectively.

Figure 15 illustrates the joint torque curves determined by simulation. By comparing joint torque curves in the non-load-carrying and load-carrying conditions we can conclude that the outputs of torque and power in the hip and the knee have great changes in both directions, while in the negative direction the ankle torque and power remains unchanged. Therefore the actuators were placed in the hip and the knee.

5.2. Load-carrying simulation with exoskeleton

During the simulation, the interactions between the exoskeleton and the human legs need to be defined in advance. In order to meet this need, springs are added between the exoskeleton and the legs. . Thus, the interactions can be represented by measuring the spring force, and the control method described above is used to implement the co-simulation. Figure 16 illustrates the walking animation of the human body model wearing the exoskeleton in the load-carrying condition.

In order to further analyze the effects of the exoskeleton on the lower limb joints, the joint torque in two situations are compared: I) Non load-carrying, no exoskeleton and II) Load-carrying, with exoskeleton. The results are shown in Figure 17.

Through the comparison scenario we determined that there is only slight variation between the two situations. The curve indicates that the exoskeleton bears the majority of the load, rather than the human. Accordingly, it further validates the remarkable assisted effect of the exoskeleton.

6. Conclusion

To conclude, we proposed a method to implement the lower limb exoskeleton. Based on the biomechanical simulation software LifeModeler, the human model was built and the movement data of each joint was obtained. We then developed the control strategy to control the contact force between the exoskeleton and the human models. Finally, the simulation results proved that the assisted effect of the exoskeleton designed in this paper is significant.

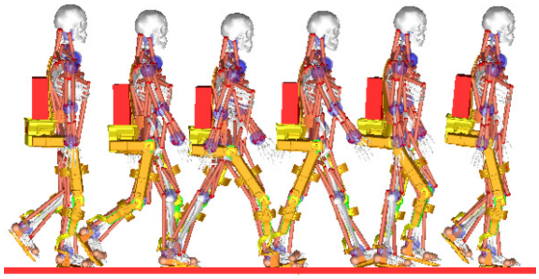

Fig. 16. The load-carrying walking illustration of the human body model with exoskeleton.

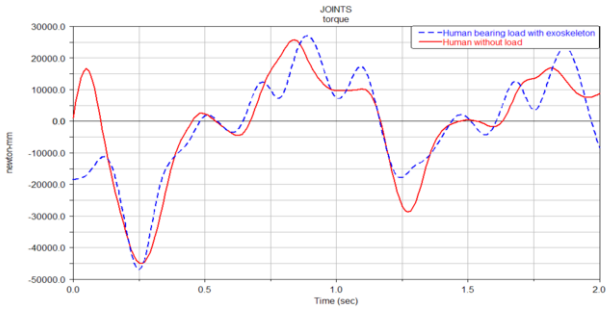

(a) Hip torque curve contrast.

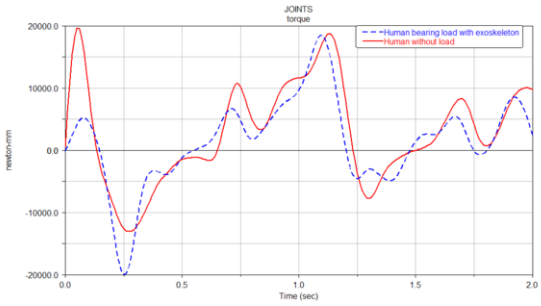

(b) Knee torque curve contrast.

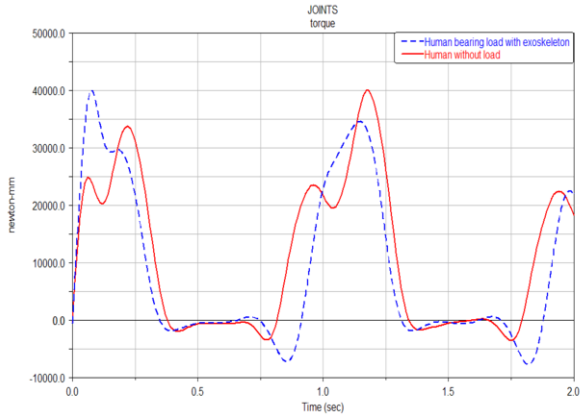

(c) Ankle torque curve contrast.

Fig. 17. The solid line represents situation I) and the dotted line represents situation II).

In our future work, the aspects of improvement include: I) The further optimization of the exoskeleton structure; II) Promotion of the anti-interference ability of the sensing system; III) Further development of the control strategy to increase its accuracy and stability; IV) To improve and perfect the experimental platform and conduct further specific-wear experiments.

Acknowledgment

The work reported in this paper is funded by the National High Technology Research and Development Program of China (863 Program, Grant No. 2012AA041505) and Support by Self-Planned Task (NO.SKLRS201501A02) of State Key Laboratory of Robotics and System (HIT).

References

[1] H.D. Lee, S.N. Yu, S. Lee, et al., Development of human-robot interfacing method for assistive wearable robot of the human upper extremities, IEEE 2008 SICE Annual Conference, 2008, pp. 1755-1760.
[2] W. Kim, S. Lee, M. Kang, et al., Energy-efficient gait pattern generation of the powered robotic exoskeleton using DME, IEEE/RSJ International Conference on Intelligent Robots and Systems (IROS), 2010, pp. 2475-2480.
[3] A. Merlo, M. Longhi, E. Giannotti, et al., Upper limb evaluation with robotic exoskeleton, normative values for indices of accuracy, speed and smoothness, NeuroRehabilitation **33** (2013), 523-530.
[4] C. Copilusi, M. Ceccarelli, N. Dumitru and G. Carbone, Design and simulation of a leg exoskeleton linkage for a human rehabilitation system, 11th IFToMM International Symposium on Science of Mechanisms and Machines, Mechanisms and Machine Science **18** (2014), 117-125.
[5] R.J. Farris, H.A. Quintero, S.A. Murray, et al., A preliminary assessment of legged mobility provided by a lower limb exoskeleton for persons with paraplegia, IEEE Neural Systems and Rehabilitation Engineering, 2014, pp. 482-490.
[6] J. Zhu and H. Zhou, Realization of key technology for intelligent xxoskeleton load xystem, In: Advances in Information Technology and Industry Applications, Springer Berlin Heidelberg, 2012, pp. 77-82.
[7] J. Okamura, H. Tanaka and Y. Sankai, EMG-based prototype powered assistive system for walking aid, Proc. Asian Symposium on Industrial Automation and Robotics, Bangkok, Thailand, 2009, pp. 229-234.
[8] S. Lee and Y. Sankai, Power assist control for walking aid with hal-3 based on EMG and impedance adjustment around knee joint, Proc. of IEEE/RSJ International Conference on Intelligent Robots and Systems, EPFL, Switzerland, 2008, pp. 1499-1504.
[9] S. Lee and Y. Sankai, Power assist control for leg with hal-3 based on virtual torque and impedance adjustment, Proc. IEEE International Conference on Systems, Man and Cybernetics (SMC), Hamm met, Tunisia, 2008.
[10] Y. Yu, W. Liang and Y. Ge, Jacobian analysis for parallel mechanism using on human walking power assisting, 2011 International Conference on IEEE Mechatronics and Automation (ICMA), 2011, pp. 282-288.
[11] Donghai Wang, Kok-Meng Lee, Jiajie Guo, et al., Adaptive knee joint exoskeleton based on biological geometries, Mechatronics, IEEE/ASME Transactions, 2014, pp. 1268-1278.
[12] S. Serveto, S. Barré, J.M. Kobus and J.P. Mariot, A three-dimensional model of the boat-oars-rower system using ADAMS and LifeMOD commercial software, Proceedings of the Institution of Mechanical Engineers, Part P, Journal of Sports Engineering and Technology **224** (2010), pp. 75-88.
[13] K.T. Huynh, et al., Simulating dynamics of thoracolumbar spine derived from LifeMOD under haptic forces, World academy of science, engineering and technology **64** (2010), 278-285.
[14] Y.S. Liu, T.S. Tsay and T.C. Wang, Muscles force and joints load simulation of bicycle riding using multibody models, Procedia Engineering **13** (2011), 81-87.
[15] Y.I. Hwang, W.G. Yoo and D.H. An, Effects of the elastic walking band on gait in stroke patients, NeuroRehabilitation **32** (2013), 317-322.
[16] G. Shuxiang, Z. Fan, W. Wei, et al., Development of force analysis-based exoskeleton for the upper limb rehabilitation syste, 2013 ICME International Conference on Complex Medical Engineering (CME), 2013, pp. 285-289.
[17] M. Baritz, D. Cotoros, L. Cristea and L. Rogozea, Assessment of human bio-behavior during gait process using LifeMod software, Broad Research in Artificial Intelligence and Neuroscience (BRAIN) **1** (2011), 169.